Determination of the antisymmetric part of the chemical shift anisotropy tensor via spin relaxation in nuclear magnetic resonance

Raphaël Paquin,[1,2,a),b)] Philippe Pelupessy,[1,a),c)] Luminita Duma,[1] Christel Gervais,[3] and Geoffrey Bodenhausen[1,2]

[1]*Département de Chimie, UMR 7203 CNRS, Ecole Normale Supérieure, 24 rue Lhomond, 75231 Paris Cedex 05, France*

[2]*Institut des Sciences et Ingénierie Chimiques, Ecole Polytechnique Fédérale de Lausanne, Batochime, 1015 Lausanne, Switzerland*

[3]*Laboratoire de Chimie de la Matière Condensée de Paris, UMR 7574 CNRS, Université Pierre et Marie Curie (Paris 6), Place Jussieu, 75005 Paris, France*

(Received 29 November 2009; accepted 14 May 2010; published online 16 July 2010)

Relaxation processes induced by the antisymmetric part of the chemical shift anisotropy tensor (henceforth called anti-CSA) are usually neglected in NMR relaxation studies. It is shown here that anti-CSA components contribute to longitudinal relaxation rates of the indole ^{15}N nucleus in tryptophan in solution at different magnetic fields and temperatures. To determine the parameters of several models for rotational diffusion and internal dynamics, we measured the longitudinal relaxation rates $R_1=1/T_1$ of ^{15}N, the ^{15}N–^{1}H dipole-dipole (DD) cross-relaxation rates (Overhauser effects), and the cross-correlated CSA/DD relaxation rates involving the second-rank symmetric part of the CSA tensor of ^{15}N at four magnetic fields $B_0=9.4$, 14.1, 18.8, and 22.3 T (400, 600, 800, and 950 MHz for protons) over a temperature range of $270<T<310$ K. A good agreement between experimental and theoretical rates can only be obtained if the CSA tensor is assumed to comprise first-rank antisymmetric (anti-CSA) components. The magnitude of the hitherto neglected antisymmetric components is of the order of 10% of the CSA. © *2010 American Institute of Physics*. [doi:10.1063/1.3445777]

I. INTRODUCTION

Chemical shifts and their modulations induced by rotational diffusion and internal motions can be exploited to investigate structural and dynamic properties of molecules.[1–3] Knowledge of chemical shift tensors is essential to characterize accurately internal dynamics at atomic resolution[4–9] or domain motions in proteins[10] or RNAs.[11] Chemical shifts reflect local magnetic fields induced by the motions of electrons surrounding a nucleus in the presence of an external static magnetic field. These electron-induced fields depend on the local electronic structure and on the orientations of molecular orbitals relative to the static magnetic field and can be described by a chemical shift tensor. Without loss of generality, this tensor can be split into three tensors of ranks $l=0$, 1, and 2, which correspond to the isotropic, anisotropic antisymmetrical, and anisotropic symmetrical parts[12]

$$\begin{pmatrix} \delta_{xx} & \delta_{yx} & \delta_{zx} \\ \delta_{xy} & \delta_{yy} & \delta_{zy} \\ \delta_{xz} & \delta_{yz} & \delta_{zz} \end{pmatrix} = \underset{l=0}{\delta_{\mathrm{iso}}\begin{pmatrix} 1 & 0 & 0 \\ 0 & 1 & 0 \\ 0 & 0 & 1 \end{pmatrix}} + \underset{l=1}{\begin{pmatrix} 0 & \delta_{xy}^{(a)} & \delta_{xz}^{(a)} \\ -\delta_{xy}^{(a)} & 0 & \delta_{yz}^{(a)} \\ -\delta_{xz}^{(a)} & -\delta_{yz}^{(a)} & 0 \end{pmatrix}} + \underset{l=2}{\begin{pmatrix} \delta_{xx}^{(s)}-\delta_{\mathrm{iso}} & \delta_{xy}^{(s)} & \delta_{xz}^{(s)} \\ \delta_{xy}^{(s)} & \delta_{yy}^{(s)}-\delta_{\mathrm{iso}} & \delta_{yz}^{(s)} \\ \delta_{xz}^{(s)} & \delta_{yz}^{(s)} & \delta_{zz}^{(s)}-\delta_{\mathrm{iso}} \end{pmatrix}}. \quad (1)$$

The zeroth-rank tensor ($l=0$), which is invariable under rotations, leads to the isotropic chemical shift $\delta_{\mathrm{iso}}=(\delta_{xx}+\delta_{yy}+\delta_{zz})/3$. The components of the first-rank ($l=1$) antisymmetric chemical shift anisotropy (henceforth anti-CSA) tensor can be expressed by $\delta_{ij}^{(a)}=(\delta_{ij}-\delta_{ji})/2$, while the second-rank ($l=2$) symmetric part of the CSA tensor (sym-CSA) components are proportional to $\delta_{ij}^{(s)}=(\delta_{ij}+\delta_{ji})/2$. The sym-CSA tensor is usually represented by its three eigenvalues in the principal axis system and the orientations of its three principal axes with respect to the molecular frame.[12] In liquids, the anisotropic parts are averaged out by rotational diffusion so that only δ_{iso} can be observed in the spectra, while the anisotropic parts give rise to relaxation. In solids, only the eigenvalues and orientations of the sym-CSA tensor can be

[a)]Authors to whom correspondence should be addressed.
[b)]Tel.: +0033 (0)1 44 32 32 65. Electronic mail: raphael.paquin@ens.fr.
[c)]Tel.: +0033 (0)1 44 32 33 44. Electronic mail: philippe.pelupessy@ens.fr.

determined. Due to the absence of diagonal elements, the anti-CSA tensor only leads to magnetic field components that are perpendicular to the main external field, regardless of the frame of reference. This results in very weak tilt of the local field and hence to a second-order contribution to the resonance frequency that is too small to be measured. Graphical illustrations of these properties can be found in Anet's reviews.[13] Just like the magnetic field components due to the sym-CSA tensor, the fields associated with the anti-CSA tensor are modulated by rotational diffusion and internal molecular motions so that they also contribute to relaxation.[14–16]

Experimental studies of the effect of anti-CSA tensor components on relaxation were carried out for some molecules with unusual electronic structures such as cyclopropenone[17] and tetrachlorocyclopropene.[18] A theoretical study by Kowalewski and Werbelow[19] addressed the contributions to the longitudinal and transverse relaxation rates R_1 and R_2 induced by the anti-CSA components of ^{15}N in formamide, where rapid anisotropic rotational diffusion exacerbates the contributions of anti-CSA tensor components to the relaxation rates.[19] In solid-state NMR, anti-CSA tensor components could be detected through a second-order shift in the presence of large quadrupolar interactions.[20]

As shown by Buckingham, the symmetry of nuclear sites limits the number of independent components of the CSA tensor.[21] Antisymmetric components only exist at sites with low nuclear symmetry (e.g., C_1, C_2, and C_S), which may occur in biomolecules such as proteins and nucleic acids. Due to the increasing popularity of very high static magnetic fields in NMR studies of biomolecules, the effects of anti-CSA tensor components become a topical issue, since the contribution of the CSA (including its anti-CSA component) to relaxation is proportional to the square of the static field. When CSA tensors can be obtained both from solid-state[22,23] and solution[24] NMR, it is important to have an estimate of the contributions of the anti-CSA components to relaxation rates in liquids since they can be a source of discrepancies.

In this work, we show an experimental investigation of the anti-CSA tensor components of the indole ^{15}N nucleus in tryptophan. While the longitudinal relaxation rate R_1 is affected by anti-CSA components, the cross-correlated CSA/DD relaxation rates and the dipole-dipole (DD) cross-relaxation rates are not. A careful comparison of these rates at different static fields and temperatures, combined with a suitable description of anisotropic rotational diffusion, allows one to assess the anti-CSA tensor components of the ^{15}N nucleus.

II. THEORY

A. The CSA tensor of indole ^{15}N in tryptophan

As shown in Fig. 1, the ^{15}N indole nucleus lies in the plane of the indole ring of tryptophan and is therefore characterized by a C_S point-group symmetry. According to Buckingham and Anet,[13,21] the sym-CSA tensor can therefore have three unlike eigenvalues δ_{xx}, δ_{yy}, and δ_{zz}, but the anti-CSA tensor can only have one unique component $\delta_{yz}^{(a)}$ perpendicular to the indole ring plane. As shown in Table I, solid-state NMR measurements[25] confirm this for the sym-CSA tensor.

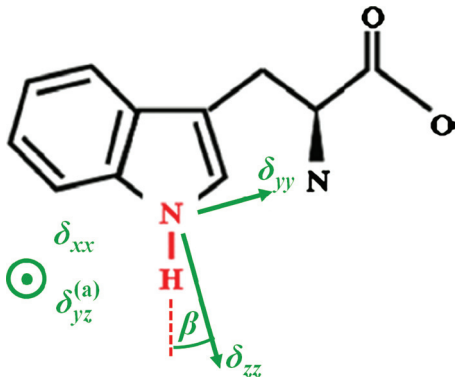

FIG. 1. The principal components and orientations of the principal axes (green) of the sym-CSA tensor of indole ^{15}N in tryptophan. The principal components (eigenvalues) are defined so that $\delta_{xx} < \delta_{yy} < \delta_{zz}$, where δ_{zz} is the least shielded component. According to a solid-state NMR study (Ref. 25), δ_{xx} lies perpendicular to the indole ring plane, while δ_{zz} lies in the indole plane and forms an angle $\beta = 5 \pm 2°$ with respect to the r_{NH} vector (red). The unique anti-CSA tensor component $\delta_{yz}^{(a)}$ is normal to the indole ring, parallel to δ_{xx}.

The most shielded CSA component δ_{xx} lies perpendicular to the indole ring, while the least shielded δ_{zz} component lies in this plane and forms an angle $\beta = 5 \pm 2°$ with respect to the r_{NH} vector.[25] Independent results obtained in our laboratory for the L-enantiomer, through the analysis of the spinning sidebands obtained at low-frequency magic angle spinning (MAS) with the DMFIT program,[26] are consistent with the earlier study[25] (Table I). We have calculated the sym-CSA and anti-CSA tensors (Table I) with Kohn–Sham density functional theory using the QUANTUM-ESPRESSO code[27] that employs the Gauge Including Projector Augmented Waves (GIPAW) method[28] and the crystal structure of DL-tryptophan determined by x-ray diffraction.[29] Details about the computations are reported elsewhere.[30,31] The calculated sym-CSA tensor components δ_{xx} and δ_{yy} are very close to the experimental results, although δ_{zz} is overestimated by ~8%. The calculated anti-CSA tensor has one major component $\delta_{yz}^{(a)}$ normal to the indole ring plane and two minor in-plane components, in rough agreement with expectations based on the molecular symmetry. The discrepancy for the eigenvalue δ_{zz} might stem from internal motions, imperfections in the crystal lattice, or inaccuracy of the DFT approach. In our study in solution, we shall assume that only the $\delta_{yz}^{(a)}$ component of the anti-CSA tensor contributes to the relaxation rates.

B. Theoretical expressions of relaxation rates

For a system with two spins $I = \frac{1}{2}$ and $S = \frac{1}{2}$ (e.g., ^{1}H and ^{15}N, simply denoted H and N in the expressions for the relaxation rates), there are three separate contributions to the longitudinal (autorelaxation) rate $R_1 = 1/T_1$ of ^{15}N arising from the second-rank ^{1}H–^{15}N DD interaction, the second-rank sym-CSA ^{15}N tensor, and the first-rank anti-CSA ^{15}N tensor,

$$R_1 = R_1^{DD} + R_1^{\text{sym-CSA}} + R_1^{\text{anti-CSA}}, \tag{2}$$

where

TABLE I. Principal components of the CSA tensor and orientations of the indole ^{15}N in the amino-acid tryptophan determined experimentally and by *ab initio* calculations. The experimental distance r_{NH} has been determined from measurements of the $^{1}H-^{15}N$ dipolar coupling (Ref. 25). Note the agreement between the published measurements and ours.

	Sym-CSA (ppm)			Anti-CSA (ppm)				
	δ_{xx}	δ_{yy}	δ_{zz}	$\delta_{xy}^{(a)}$	$\delta_{xz}^{(a)}$	$\delta_{yz}^{(a)}$	β (°)	r_{NH} (Å)
Solid-state NMR[a]	61.0 ± 1	129.6 ± 1	180.8 ± 1	⋯	⋯	⋯	5 ± 3	1.06 ± 0.02
Solid-state NMR (this work)	61.2	126.4	182.2	⋯	⋯	⋯	⋯	⋯
Calculated (this work)	60.2	129.4	195.8	0.84	−1.78	7.96	⋯	⋯

[a]Reference 25.

$$R_1^{DD}=(c_{NH})^2\{2J^{(2)}_{NH,NH}(\omega_H-\omega_N)+6J^{(2)}_{NH,NH}(\omega_N)+12J^{(2)}_{NH,NH}(\omega_H+\omega_N)\}, \quad (3)$$

$$R_1^{sym\text{-}CSA}=(c_N)^2\{6(\delta_{zz}-\delta_{xx})^2J^{(2)}_{zz,zz}(\omega_N)+6(\delta_{yy}-\delta_{xx})^2J^{(2)}_{yy,yy}(\omega_N)+12(\delta_{zz}-\delta_{xx})(\delta_{yy}-\delta_{xx})J^{(2)}_{zz,yy}(\omega_N)\}, \quad (4)$$

and[14,16,19]

$$R_1^{anti\text{-}CSA}=3(c_N)^2(\delta_{yz}-\delta_{zy})^2\{5/2J^{(1)}_{xx,xx}(\omega_N)\}, \quad (5)$$

where $c_N=\omega_N\sqrt{2}/6$, $c_{NH}=\mu_0\hbar\gamma_N\gamma_H\sqrt{2}/(16\pi r_{NH}^3)$, μ_0 is the permeability of free space, $\hbar$ is Planck's constant divided by 2π, γ_N and γ_H are the gyromagnetic ratios of ^{15}N and ^{1}H, r_{NH} is the distance between ^{15}N and ^{1}H, and $J^{(l)}_{uv}$ are spectral densities, which result from the Fourier transformation of autocorrelation functions of rank $l=1$ or 2, characterized by correlation times $\tau_c^{(l)}$ of rank l. We define the fraction f of longitudinal relaxation induced by anti-CSA as

$$f=R_1^{anti\text{-}CSA}/(R_1^{DD}+R_1^{sym\text{-}CSA}+R_1^{anti\text{-}CSA}). \quad (6)$$

Note that this fraction would increase if the neighboring ^{1}H were replaced by a deuteron since $\gamma_D \ll \gamma_H$.

The $^{15}N-^{1}H$ DD cross-relaxation rate (nuclear Overhauser effect) is

$$\sigma_{NH}^{NOE}=(c_{NH})^2\{12J^{(2)}_{NH,NH}(\omega_H+\omega_N)-2J^{(2)}_{NH,NH}(\omega_H-\omega_N)\}. \quad (7)$$

The longitudinal R_{ccl} and transverse R_{cct} cross-correlated CSA/DD rates are[32]

$$R_{ccl}=-12c_Nc_{NH}\{(\delta_{zz}-\delta_{xx})J^{(2)}_{zz,NH}(\omega_N)+(\delta_{yy}-\delta_{xx})J^{(2)}_{yy,NH}(\omega_N)\}, \quad (8)$$

$$R_{cct}=-2\,c_Nc_{NH}\{(\delta_{zz}-\delta_{xx})(3J^{(2)}_{zz,NH}(0)+4J^{(2)}_{zz,NH}(\omega_N)+(\delta_{yy}-\delta_{xx})(3J^{(2)}_{yy,NH}(0)+4J^{(2)}_{yy,NH}(\omega_N)\}. \quad (9)$$

The spectral densities $J^{(l)}_{uv}$ express the combined effect of two interactions u and v (for example, CSA and DD interactions) and depend on the angles subtended by the symmetry axes of the tensors.

C. Model A: Isotropic rotational diffusion without internal motions

For isotropic rotational diffusion without internal motions, the spectral density function can be expressed as

$$J^{(l)}_{uv}(\omega)=\frac{2}{5}P_{(l)}(\cos\,\theta_{uv})\frac{\tau_c^{(l)}}{1+(\omega\tau_c^{(l)})^2}, \quad (10)$$

where $\tau_c^{(l)}$ is the rotational correlation time for interactions of rank l. For isotropic diffusion, one has the relation $\tau_c^{(1)}=3\tau_c^{(2)}$.[16] Note that $\tau_c^{(2)}$ is the correlation time τ_c encountered in conventional NMR relaxation studies where second-rank interactions (i.e., sym-CSA and DD interactions) play a predominant role. $P_{(l)}$ is the Legendre polynomial of order l [$P_1[x]=x$ and $P_2[x]=(3x^2-1)/2$], and θ_{uv} are the angles between the principal axes of the DD or CSA interactions involved. For isotropic rotational diffusion $\tau_c=\tau_c^{(2)}$,

$$J^{1}_{uv}(\omega)=\frac{2}{5}P_1(\cos\,\theta_{uv})\frac{3\tau_c}{1+\omega^2(3\tau_c)^2}. \quad (11)$$

For the orientation in Fig. 1, the angles between the principal axes of the CSA and DD interactions are $\theta_{xx,NH}=\pi/2$, $\theta_{zz,NH}=\beta$, and $\theta_{yy,NH}=\pi/2-\beta$.

D. Model B: Isotropic rotational diffusion with internal motions

To take into account the internal motions in addition to isotropic overall tumbling, the Lipari–Szabo formalism[33] can be used

$$J^{(l)}_{uv}(\omega)=\frac{2}{5}\left[S^{2(l)}_{uv}\frac{\tau_c^{(l)}}{1+(\omega\tau_c^{(l)})^2}+\{P_{(l)}(\cos\,\theta_{uv})-S^{2(l)}_{uv}\}\times\frac{\tau_{eff}^{(l)}}{1+(\omega\tau_{eff}^{(l)})^2}\right], \quad (12)$$

with $1/\tau_{eff}^{(l)}=1/\tau_c^{(l)}+1/\tau_{int}^{(l)}$, where $\tau_{int}^{(l)}$ of rank l is the effective correlation time of the internal motions, and the order parameter $S^{2(l)}_{uv}$ of rank l characterizes the amplitude of these motions. The internal motions are assumed to be isotropic in the sense that the amplitudes of the angular fluctuations of a vector are independent of its orientation with respect to the molecular frame, i.e., $S^{2(l)}_{uv}=S^{2(l)}P_{(l)}(\cos\,\theta_{uv})$. Here again, the condition $\tau_c^{(1)}=3\tau_c^{(2)}$ holds. For internal motions with small

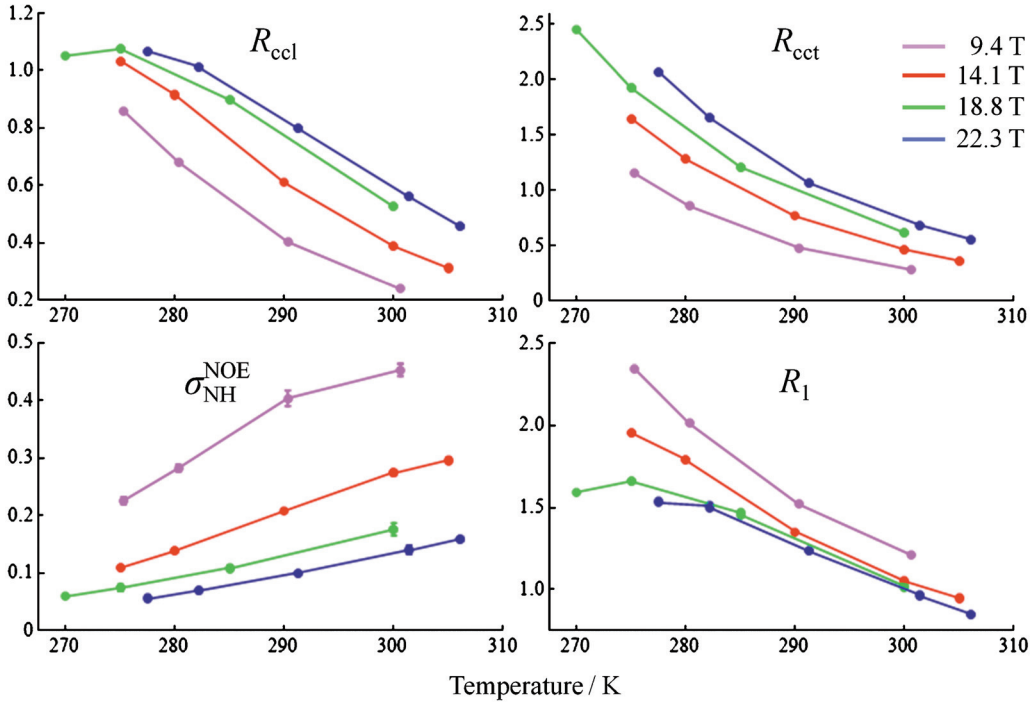

FIG. 2. Autocorrelated longitudinal relaxation rates $R_1(^{15}N)$, dipolar cross-relaxation rates σ_{NH}^{NOE} ($^1H \rightarrow ^{15}N$), and cross-correlated transverse R_{cct} and longitudinal R_{ccl} relaxation rates due to concerted fluctuations of the symmetrical CSA(^{15}N) and DD($^{15}N-^1H$) interaction, measured at $B_0=9.4$ T (magenta), 14.1 T (red), 18.79 T (green), and 22.32 T (blue) for temperatures in the range of $270<T<310$ K.

amplitudes, the relations $\tau_{int}^{(1)}=\tau_{int}^{(2)}$ and $S^{2(l=1)}=2/3+S^{2(l=2)}/3$ can be obtained by a Taylor expansion to the second order of the Legendre polynomials.

E. Model C: Anisotropic rotational diffusion without internal motions

For the sake of simplicity, the rotational diffusion tensor will be assumed to be axially symmetric with $D_\parallel \neq D_\perp$ and internal motions are neglected ($S^2=1$). The spectral density function obtained by Fourier transformation of the second-rank autocorrelation function is then

$$J_{uv}^{(2)}(\omega)=\frac{2}{5}\sum_{j=0}^{2}\frac{A_j\tau_j^{(2)}}{1+(\omega\tau_j^{(2)})^2}, \tag{13}$$

where $1/\tau_j^{(2)}=6D_\perp-j^2(D_\perp-D_\parallel)$ and

$$A_0=(3\cos^2\theta_u^d-1)(3\cos^2\theta_v^d-1)/4,$$

$$A_1=3\sin\theta_u^d\cos\theta_u^d\sin\theta_v^d\cos\theta_v^d\cos\phi_{uv}^d, \tag{14}$$

$$A_2=(3/4)\sin^2\theta_u^d\sin^2\theta_v^d\cos 2\phi_{uv}^d,$$

where $\phi_{uv}^d=\phi_u^d-\phi_v^d$. The polar and azimuthal angles θ_u^d, θ_v^d, ϕ_u^d, and ϕ_v^d define the orientations of the eigenvectors of the sym-CSA tensor and the anti-CSA tensor components with respect to the diffusion frame. For isotropic tumbling, i.e., for $D_\perp=D_\parallel$, one finds again $\tau_j^{(2)}=\tau_c$.

The antisymmetric spectral density is[16]

$$J_{uv}^{(1)}(\omega)=\frac{2}{5}P_1(\cos\theta_{uv})\left[\cos(\phi_{yz}^d)^2\sin(\theta_{yz}^d)^2\frac{\tau_{j=0}^{(1)}}{1+(\omega\tau_{j=0}^{(1)})^2}+\{\sin(\phi_{yz}^d)^2+\cos(\phi_{yz}^d)^2\cos(\theta_{yz}^d)^2\}\frac{\tau_{j=1}^{(1)}}{1+(\omega\tau_{j=1}^{(1)})^2}\right], \tag{15}$$

where $1/\tau_j^{(l)}=2D_\perp-j^2(D_\perp-D_\parallel)$. Note that for isotropic diffusion ($D_\perp=D_\parallel$ and $\tau_{j=0}^{(1)}=\tau_{j=1}^{(1)}=3\tau_c$), we retrieve Eq. (11).

III. EXPERIMENTS

L-tryptophan, enriched in ^{15}N (Fig. 1), was dissolved in a mixture of 90% ethylene glycol and 10% H_2O. D_2O was used as an external lock in an inner concentric tube. The viscosity of ethylene glycol is 18 times larger than that of water at 293 K, and its melting point is $T_{mp}\sim 260$ K so that a wide range of rotational diffusion regimes can be probed.

The ^{15}N longitudinal autorelaxation rates R_1 were measured using a conventional out and back sequence[34] with relaxation delays $T_R=0.2$, 0.4, 0.5, 0.6, 0.8, 1.0, 1.25, and 1.5 s. The symmetrical reconversion approach[35,36] was used to measure the longitudinal CSA/DD cross-correlation rates (R_{ccl}) with delays $T_R=0.16$, 0.33, 0.49, 0.66, and 0.99 s and the transverse CSA/DD cross-correlation rates (R_{cct}) with delays $T_R=0.04$, 0.08, 0.12, 0.16, 0.20, and 0.24 s. To determine the σ_{NH}^{NOE} cross-relaxation ($^1H \rightarrow ^{15}N$) rates, we used the steady-state NOE scheme recently proposed by Ferrage *et al.*,[37,38] based on symmetric saturation[37] combined with π pulses.[38] Experiments were performed at four static fields $B_0=9.4$ T (400 MHz), 14.1 T (600 MHz), 18.79 T (800 MHz), and 22.32 T (950 MHz) for temperatures

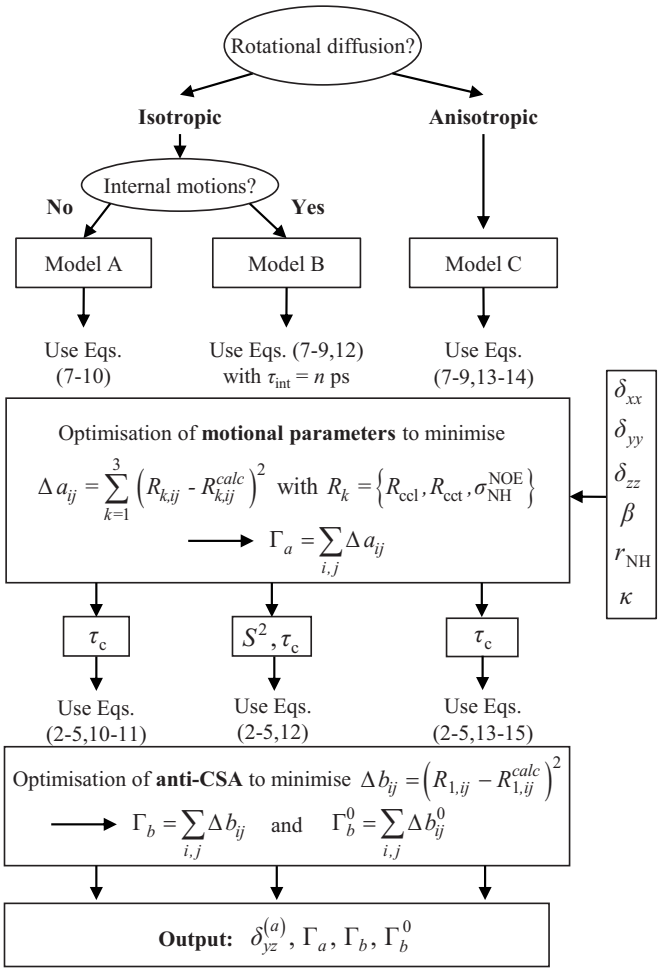

FIG. 3. Data fitting strategies employed to assess the anti-CSA contribution to R_1 rates, i.e., the anti-CSA component $\delta_{yz}^{(a)}$. Details about the three approaches are given in the text: isotropic diffusion without (model A) or with internal motions (model B) and anisotropic diffusion without internal motions (model C). The indices i and j represent the static field B_{0i}=9.4, 14.1, 18.79, and 22.32 T and the temperature $270 < T_j < 310$ K.

$270 < T < 310$ K (Fig. 2). The difference between the chemical shifts of the ethylene glycol protons served as an internal thermometer.[39] More details about the experiments (relaxation curves, rates, and techniques used to control the temperature) are given in the supplementary material.[40]

IV. ANALYSIS

The cross-correlation and cross-relaxation rates $R_k = \{R_{ccl}, R_{cct}, \sigma_{NH}^{NOE}\}$, which do not depend on anti-CSA components (unlike the autorelaxation rates R_1), were used to fit the motional parameters, i.e., the second-rank correlation times $\tau_c^{(2)}$ and $\tau_j^{(2)}$ and the order parameter S^2 at each temperature and magnetic field, following a fitting procedure outlined in Fig. 3. The best parameters lead to the smallest deviations $\Delta a_{ij} = \Sigma_{k=1}^{3} (R_{k,ij} - R_{k,ij}^{calc})^2$ for the three rates $R_k = \{R_{ccl}, R_{cct}, \sigma_{NH}^{NOE}\}$, which are assumed to have equal accuracy. The index i stands for the different static fields B_{0i} and j for the different temperatures T_j. Contrary to the commonly used minimization of χ^2 functions, the relaxation rates R_k were not weighted by their errors to avoid attributing unreasonably large weights to rates that have small random errors. In fact, for some of the rates, the stochastic variations of the data points were so small (less than 0.1% at the higher fields) that systematic errors inherent to the experiments are probably dominant. Such systematic errors could, for example, be due to pulse imperfections, small errors in the temperature calibration (<0.1 K), or imperfect averaging of different pathways in cross-correlation experiments. A classical χ^2 fit (where the rates are weighted by the inverse of their uncertainties) leads to parameters that lie within the error bars of the results presented here. The sum $\Gamma_a = \Sigma_{i,j} \Delta a_{ij}$ characterizes the overall deviation of the three relaxation rates that do *not* depend on anti-CSA components.

TABLE II. Estimates of the anti-CSA component $\delta_{yz}^{(a)}$ derived from the discrepancy between R_1 and $R_k = \{R_{ccl}, R_{cct}, \sigma_{NH}^{NOE}\}$, assuming isotropic rotational diffusion without internal motions (model A) and various orientations of the principal values of the sym-CSA tensor with respect to the vector r_{NH}. The CSA eigenvalues obtained in our laboratory were combined with $\beta = 5°$ and $r_{NH} = 1.06$ Å.

Model A: Isotropic rotational diffusion without internal motions				
	$\delta_{yz}^{(a)}$ (ppm)	Γ_a	Γ_b	Γ_b^0
Using CSA parameters from Ref. 25	11.72 ± 2.95	0.0117	0.0019	0.0141
$r_{NH} = 1.04$ Å	0 ± 0	0.0889	0.3072	0.3072
$r_{NH} = 1.08$ Å	31.95 ± 9.40	0.0386	0.1610	0.4447
$\beta = 3°$	12.53 ± 2.87	0.0134	0.0020	0.0170
$\beta = 7°$	10.17 ± 3.77	0.0099	0.0023	0.0106
Using our own CSA parameters	15.35 ± 5.69	0.0325	0.0075	0.0407

Next, the motional parameters thus extracted were used to determine the anti-CSA contribution to the longitudinal relaxation rate R_1. The anti-CSA tensor component $\delta_{yz}^{(a)}$ was optimized to minimize $\Delta b_{ij} = (R_{1,ij} - R_{1,ij}^{calc})^2$ over the ensemble of all R_1 rates measured at the magnetic fields B_{0i}=9.4, 14.1, 18.79, and 22.32 T for all temperatures $270 < T_j < 310$ K. The deviation $\Gamma_b = \Sigma_{i,j} \Delta b_{ij}$ is smallest for the best value of $\delta_{yz}^{(a)}$. For comparison, we also calculated $\Gamma_b^0 = \Sigma_{i,j} \Delta b_{ij}^0$ obtained if one purposely assumed that $\delta_{yz}^{(a)} = 0$, i.e., that the CSA tensor is symmetric.

Estimates of the eigenvalues of the sym-CSA tensors and assumptions about the distance r_{NH} obviously affect the motional parameters and the anti-CSA contributions extracted by our fitting procedure. The repercussions of the parameters on the determination of $\delta_{yz}^{(a)}$ will be further investigated below.

A. Model A: Isotropic rotational diffusion without internal motions

The correlation times τ_c were optimized using the distance $r_{NH} = 1.06$ Å and eigenvalues of the sym-CSA tensor given in Table I. We have used the estimates derived from solid-state NMR measurements by Opella and co-workers[25] rather than our own work (Table I). Fitting leads to a significant anti-CSA component $\delta_{yz}^{(a)} = 11.72 \pm 2.95$ ppm (Table II). Figure 4 illustrates the agreement obtained between experi-

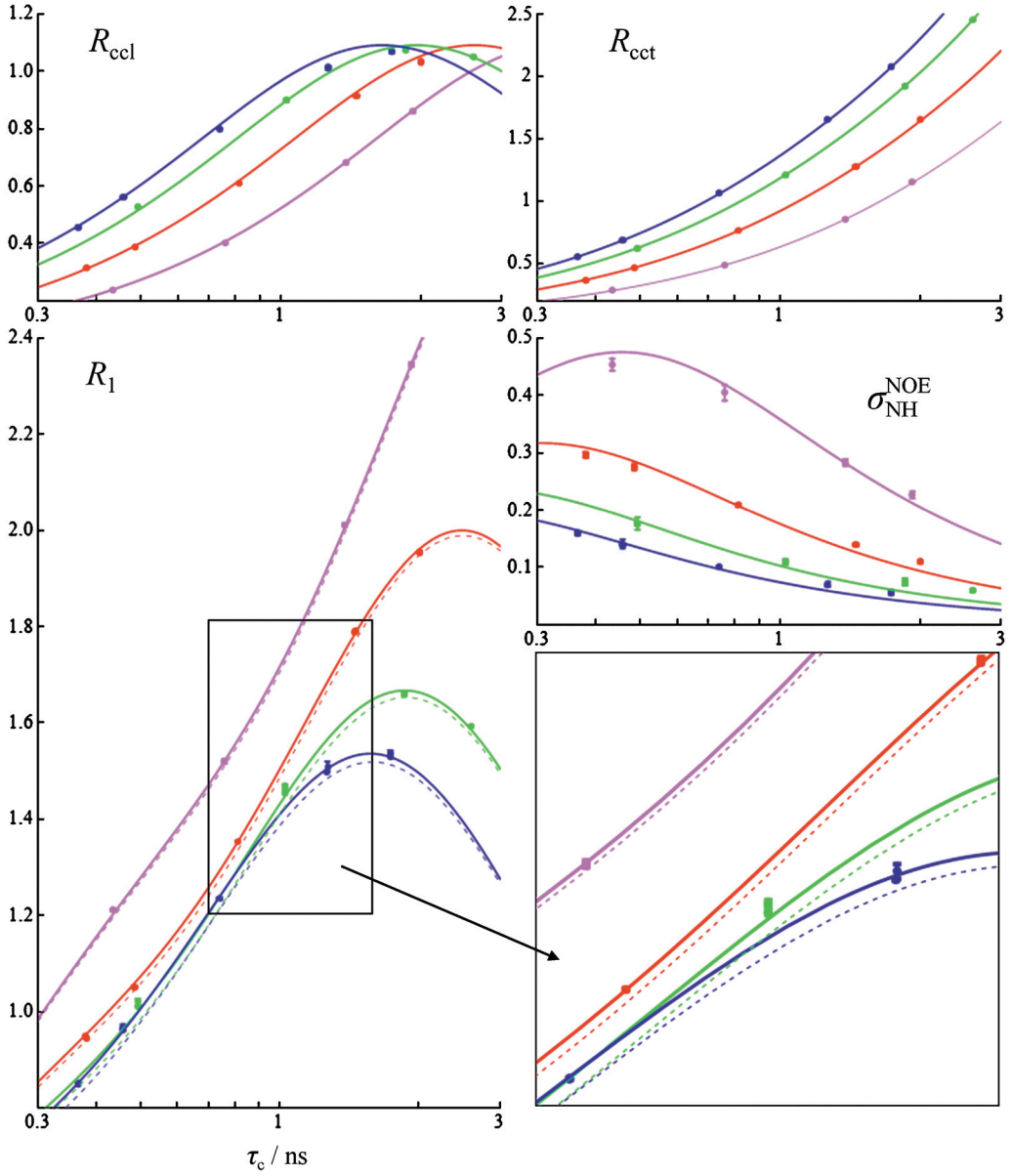

FIG. 4. Experimental and theoretical relaxation rates at 9.4 T (magenta), 14.1 T (red), 18.79 T (green), and 22.32 T (blue) vs the second-rank correlation times τ_c extracted from the isotropic rotational diffusion model without internal motions (model A) using CSA eigenvalues and a distance r_{NH} obtained by solid-state NMR (Ref. 25). The continuous and dashed lines represent the theoretical R_1 rates with or without the anti-CSA contribution, respectively.

mental and theoretical relaxation rates, confirmed by the relatively small Γ_a and Γ_b deviations. The visual assessment of the curves and the fact that if we assume, for the sake of the argument, that $\delta_{yz}^{(a)}=0$, the deviation increases considerably to $\Gamma_b^0 \sim 7\ \Gamma_b$ strongly suggest that the anti-CSA contribution to the R_1 relaxation rates is not a mere illusion.

Table II shows the anti-CSA component $\delta_{yz}^{(a)}$ and deviations obtained for several estimates of the distance r_{NH}, the angle β, and the principal values of the sym-CSA tensor. Assuming $r_{NH}=1.04$ Å rather than 1.06 Å leads to $\delta_{yz}^{(a)}=0$, but this assumption has a deleterious impact on the overall agreement between theoretical and experimental rates, as illustrated in Fig. 5(a). Variations of the eigenvectors or eigenvalues of the sym-CSA tensor have less impact, and the fits always yield a nonvanishing anti-CSA component $\delta_{yz}^{(a)}$.

We always found a nonvanishing anti-CSA component $\delta_{yz}^{(a)}$ when the overall fit of relaxation rates was acceptable, even though the magnitude of the $\delta_{yz}^{(a)}$ component depends on the distance r_{NH}, the angle β, and the sym-CSA components used as input of the fitting procedure. Further graphical results are presented in the supplementary material.[40]

B. Model B: Isotropic rotational diffusion with internal motions

As mentioned in the theoretical section, internal dynamics and anisotropic rotational diffusion must be considered to obtain unambiguous evidence of anti-CSA contributions to R_1 relaxation rates. In model B, the correlation times τ_c and order parameters S^2 have been optimized for $\tau_{int}=0$, 100, 200, and 500 ps. In all cases, the deviations Γ_a are reduced compared to the rigid model A (Table III), highlighting that the overall fit for the three rates $R_k=\{R_{ccl}, R_{cct}, \sigma_{NH}^{NOE}\}$ has

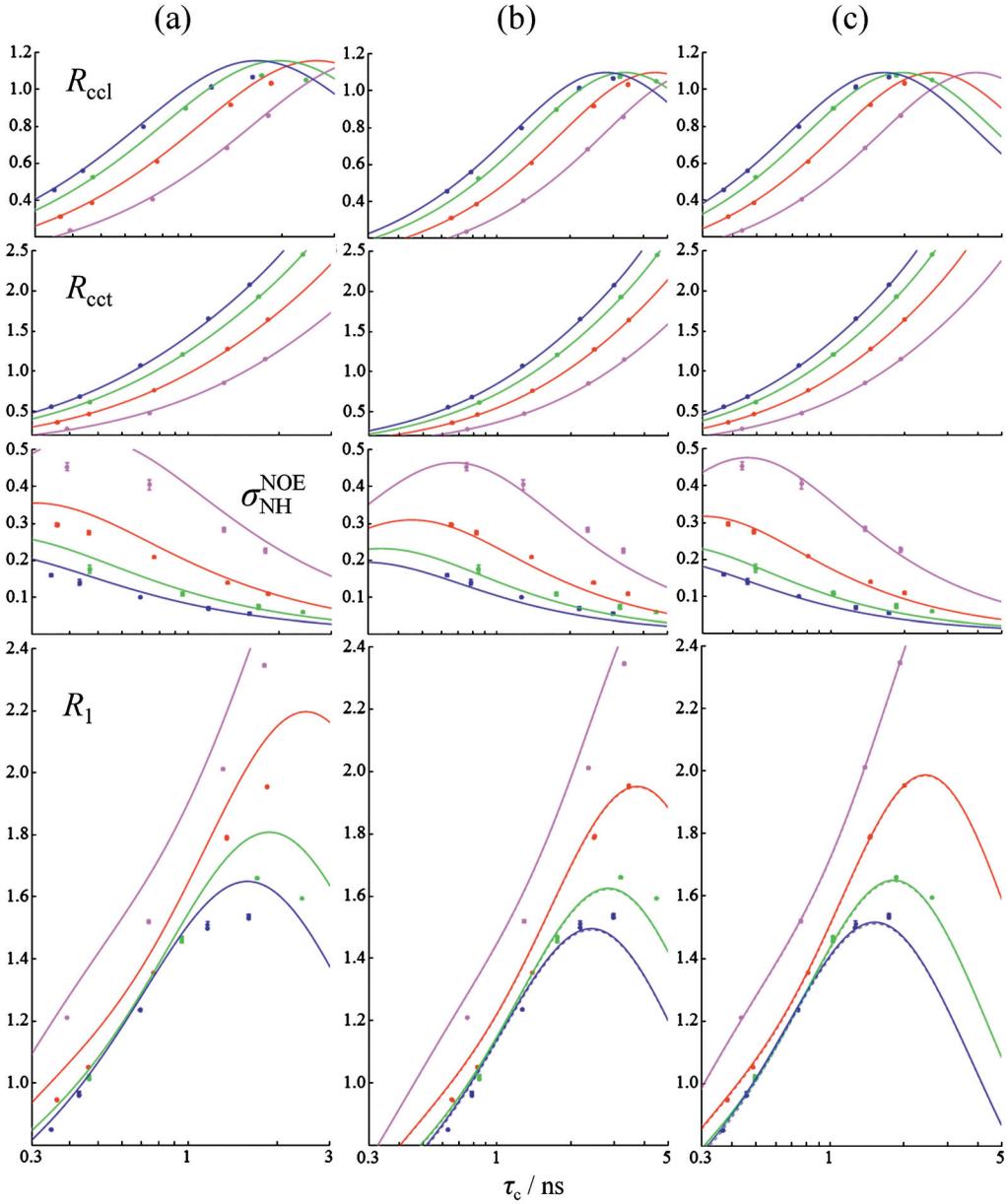

FIG. 5. Experimental and theoretical relaxation rates at 9.4 T (magenta), 14.1 T (red), 18.79T (green), and 22.32 T (blue) vs the second-rank correlation times τ_c extracted from (a) isotropic (model A) or [(b) and (c)] anisotropic (model C) rotational diffusion model. The (almost superimposed) continuous and dashed lines represent respectively the theoretical R_1 rates with or without the anti-CSA contribution. (a) $r_{NH}=1.04$ Å, [(b) and (c)] the principal axis of the diffusion tensor is collinear with (b) $D_\parallel/D_\perp=2$ and $\theta_{zz}^d=\pi/2+\beta$ or (c) $D_\parallel/D_\perp=0.5$ and $\theta_{zz}^d=\beta$.

TABLE III. Estimates of the anti-CSA component $\delta_{yz}^{(a)}$ derived from relaxation rates, assuming isotropic rotational diffusion with internal motions (model B). These results were obtained using components of the sym-CSA tensor determined by solid-state NMR (Ref. 25).

Model B: Isotropic rotational diffusion with internal motions					
	S^2	$\delta_{yz}^{(a)}$ (ppm)	Γ_a	Γ_b	Γ_b^0
$\tau_{int}=0$ ps	0.981 ± 0.016	16.76 ± 4.28	0.0053	0.0090	0.0446
$\tau_{int}=100$ ps	0.964 ± 0.028	17.11 ± 4.07	0.0035	0.0077	0.0449
$\tau_{int}=200$ ps	0.940 ± 0.051	17.00 ± 3.95	0.0027	0.0070	0.0422
$\tau_{int}=500$ ps	0.852 ± 0.149	16.93 ± 3.86	0.0021	0.0076	0.0397

been improved. The greater dispersion of the estimates of the anti-CSA component $\delta_{yz}^{(a)}$ leads to an increase of the deviations Γ_b in comparison with model A. However, Γ_b^0 is always significantly larger than Γ_b, which confirms once again that the anti-CSA contributions should not be neglected. Compared to model A, hardly any improvements of the fits could be achieved. However, this does not imply that there are no internal motions. In fact, since the effective distance r_{NH} and sym-CSA eigenvalues are also affected by internal motions when determined by solid-state NMR, these are to some extent taken into account implicitly in model A. Note that if one chooses a distance r_{NH} that is smaller in model B than in model A, one must simultaneously scale the sym-CSA eigenvalues to give an acceptable fit. The estimate of $\delta_{yz}^{(a)}$ remains positive and non-negligible.

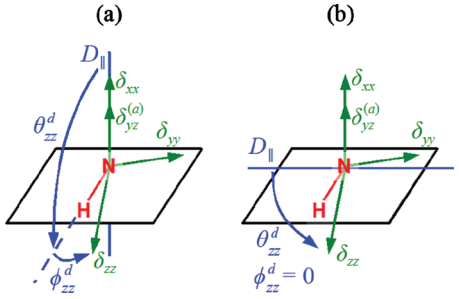

FIG. 6. The symmetry axis $D_\parallel$ of the rotational diffusion tensor could either stand perpendicular to (a) or lie in (b) the indole ring plane. The polar angles θ_{zz}^d and ϕ_{zz}^d define the orientation of the δ_{zz} component of the sym-CSA tensor with respect to $D_\parallel$ in the diffusion frame.

C. Model C: Anisotropic rotational diffusion without internal motions

As shown in Fig. 6, the symmetry axis $D_\parallel$ of the rotational diffusion tensor could either be normal to the indole ring plane [Fig. 6(a)] or lie in this plane [Fig. 6(b)]. In the former case, $D_\parallel$ is parallel to the anti-CSA component $\delta_{yz}^{(a)}$ so that $\theta_{zz}^d=\theta_{yy}^d=\theta_{\mathrm{NH}}^d=\pi/2$, $\theta_{yz}^d=0$, $\phi_{zz}^d=\beta$, $\phi_{yy}^d=\pi/2+\beta$, and $\phi_{\mathrm{NH}}^d=0$. If the symmetry axis $D_\parallel$ lies in the indole ring plane, the angles subtended between the principal axes of the sym-CSA tensor or the DD-tensor and $D_\parallel$ are $\phi_{zz}^d=\phi_{yy}^d=\phi_{\mathrm{NH}}^d=0$, $\theta_{yz}^d=0$, and $\phi_{yz}^d=\pi/2$. The remaining angles θ_{uv}^d are defined by the position of $D_\parallel$ in the plane. As presented in Table IV, several orientations can be considered, assuming, for instance, that the zz-component of the sym-CSA tensor lies in such a manner that $\theta_{zz}^d=\beta$, $\theta_{zz}^d=\pi/4+\beta$, $\theta_{zz}^d=\pi/2+\beta$, or $\theta_{zz}^d=3\pi/4+\beta$. We assume that the anisotropy $\kappa=D_\parallel/D_\perp$ of the rotational diffusion tensor in tryptophan ranges between $\kappa=0.5$ (oblate anisotropy) and $\kappa=2$ (prolate anisotropy). For a given κ, the correlation times $\tau_j^{(l)}$ can be expressed as a function of a single second-rank correlation time $\tau_{j=0}^{(2)}=\tau_c$, which is again optimized by fitting the three relaxation rates $R_k=\{R_{\mathrm{ccl}},R_{\mathrm{cct}},\sigma_{\mathrm{NH}}^{\mathrm{NOE}}\}$ that are not affected by anti-CSA components. The accuracy of the resulting anti-CSA component $\delta_{yz}^{(a)}$ can again be appreciated from the deviations Γ_b and Γ_b^0.

As shown in Table IV, assumptions about the orientation of the diffusion tensor affect the resulting anti-CSA component. If $\kappa=2$, we obtain a minimum of $\delta_{yz}^{(a)}=6.10\pm10.75$ ppm if $D_\parallel$ lies in the indole plane perpendicular to the r_{NH} vector and a maximum of $\delta_{yz}^{(a)}$ 24.97 ± 8.74 ppm if $D_\parallel$ is normal to the indole plane. The deviations Γ_b are always higher than for isotropic models, and it turns out that $\Gamma_b<\Gamma_b^0$ for each geometry, except for the case shown in Fig. 5(b), where $\theta_{zz}^d=\pi/2+\beta$ and $\kappa=2$, which lead to the largest Γ_a and Γ_b. All cases once again confirm that the anti-CSA component $\delta_{yz}^{(a)}$ cannot be neglected.

The lowest deviations Γ_a and Γ_b that can be obtained with the anisotropic diffusion model C are found when the principal axis of the diffusion tensor $D_\parallel$ is oriented parallel to the r_{NH} vector ($\theta_{zz}^d=\beta$). In this geometry, the resulting second-rank correlation times $\tau_j^{(2)}$ are not sensitive to any changes in the anisotropy κ, leading to the same deviation Γ_a as obtained for the model A. When $\kappa=0.5$, one obtains a small but poorly defined $\delta_{yz}^{(a)}=7.11\pm6.98$ ppm, with a deviation Γ_b that is as small as for the isotropic rotational diffusion model A. This might raise some doubts about the very existence of a nonvanishing anti-CSA component $\delta_{yz}^{(a)}$. However, a graphical examination of experimental and theoretical rates in Fig. 5(c) lifts these doubts. Since the anti-CSA component $\delta_{yz}^{(a)}$ appears to diminish when the correlation time increases, a good agreement for a high estimate of τ_c is reassuring. Obviously, the agreement is poor for high τ_c (low temperature) at $B_0=18.79$ and 22.32 T. Generally speaking, the lowest deviation Γ_b is found when diffusion is almost isotropic, i.e., when $D_\parallel/D_\perp\sim1$.

We tend to prefer models that not only lead to small deviations Γ_a and Γ_b, such as the isotropic rotational diffusion (model A) with $3°\leqslant\beta\leqslant7°$, $r_{\mathrm{NH}}=1.06$ Å, and experimentally determined CSA eigenvalues.[25] These assumptions yield an anti-CSA component $\delta_{yz}^{(a)}$ that is close to the results of *ab initio* calculations. Figure 7(a) shows that the fraction f of the longitudinal relaxation induced by the anti-CSA component $\delta_{yz}^{(a)}=11.72\pm2.95$ ppm ($\beta=5°$) reaches a maximum of $f=3\%$ when $\tau_c\sim0.3$ ns at $B_0=22.32$ T. For a ^{15}N nucleus with an adjacent deuteron, this ratio would increase

TABLE IV. Estimates of the anti-CSA component $\delta_{yz}^{(a)}$ derived from relaxation rates, assuming anisotropic rotational diffusion without internal motions (model C) with $D_\parallel$ either perpendicular to the indole plane or lying in this plane. These results were obtained using components of the sym-CSA tensor determined by solid-state NMR (Ref. 25).

Model C: Anisotropic rotational diffusion without internal motions						
		κ [a]	$\delta_{yz}^{(a)}$ (ppm)	Γ_a	Γ_b	Γ_b^0
$D_\parallel$ perpendicular to indole plane [Fig. 6(a)]		0.5	8.33 ± 8.73	0.0110	0.0375	0.0380
		2	24.97 ± 8.74	0.0128	0.0637	0.1967
$D_\parallel$ in-plane [Fig. 6(b)]	$\theta_{zz}^d=\beta$	0.5	7.11 ± 6.98	0.0117	0.0054	0.0066
		2	17.11 ± 2.70	0.0117	0.0034	0.0531
	$\theta_{zz}^d=\pi/2+\beta$	0.5	22.63 ± 7.97	0.0150	0.0325	0.1481
		2	6.10 ± 10.75	0.0250	0.1107	0.1030
	$\theta_{zz}^d=\pi/4+\beta$	0.5	19.01 ± 5.60	0.0075	0.0161	0.0648
		2	8.60 ± 7.45	0.0083	0.0160	0.0220
	$\theta_{zz}^d=3\pi/4+\beta$	0.5	18.55 ± 4.88	0.0070	0.0116	0.0575
		2	8.88 ± 7.02	0.0074	0.0113	0.0185

[a] $\kappa=D_\parallel/D_\perp$.

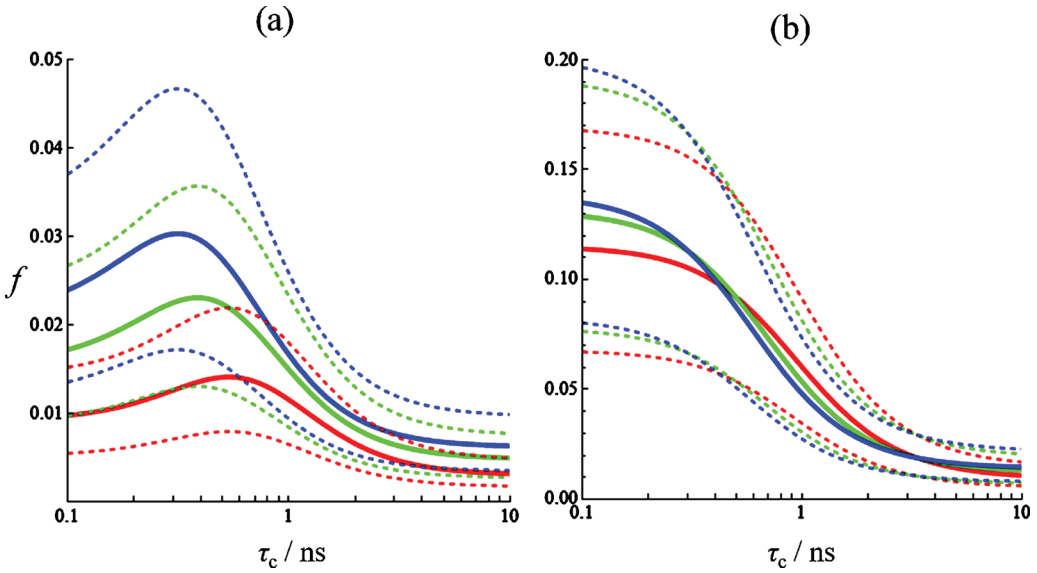

FIG. 7. Fraction f [Eq. (6)] of the longitudinal relaxation R_1 rates due to the antisymmetric part of the CSA tensor, $R_1^{\text{a-CSA}}$, vs the second-rank correlation time τ_c for isotropic reorientations at 14.1 T (red), 18.79 T (green), and 22.32 T (blue) with $\delta_{yz}^{(a)}=11.72\pm2.95$ ppm for a ^{15}N nucleus attached either (a) to ^{1}H or (b) to ^{2}H. The continuous line represents the expected proportion for the mean value $\delta_{yz}^{(a)}=11.72$ ppm, while the upper (lower) dashed lines depict the proportion for $\delta_{yz}^{(a)}=14.67\,(8.77)$ ppm, i.e., for the upper (lower) bounds of its standard deviation.

to $f=14\%$ [Fig. 7(b)]. If the proton-carrying indole ^{15}N nucleus belonged to a tryptophan residue in a globular protein tumbling with $4\leqslant\tau_c\leqslant10$ ns, this ratio would fall to a mere $f\leqslant1\%$ (for N–D; $f\leqslant2\%$) at $B_0=22.32$ T.

V. CONCLUSIONS

In this study, we have shown that the antisymmetric components of the tensors describing CSAs provide a small contribution to the autocorrelated longitudinal relaxation rates of the indole ^{15}N in tryptophan. We were able to determine the anti-CSA component $\delta_{yz}^{(a)}$ since it contributes to the autocorrelated longitudinal relaxation rate R_1, while it does not contribute to the cross-correlation and cross-relaxation rates $R_k=\{R_{\text{ccl}},R_{\text{cct}},\sigma_{\text{NH}}^{\text{NOE}}\}$. The anti-CSA contribution can be readily determined if we assume isotropic rotational diffusion of a rigid molecule. Even when intramolecular motions or anisotropic global rotational diffusion are taken into account, the rates R_1 and $R_k=\{R_{\text{ccl}},R_{\text{cct}},\sigma_{\text{NH}}^{\text{NOE}}\}$ can only be reconciled by postulating a nonvanishing anti-CSA component $\delta_{yz}^{(a)}$.

The contributions due to the anti-CSA components varied from 0.32% to 1.41% at 14.1 T (600 MHz) and from 0.67% to 3.03% at 22.32 T (950 MHz). If amide backbone nitrogen nuclei in slowly tumbling proteins have similar anti-CSA components (which remains to be shown), it would be important to take these components into consideration whenever the precision of the measurements is better than 1% at 950 MHz. This level of precision can indeed be achieved[24,41,42] but hardly in routine experiments.

It would be interesting to repeat the experiments for a case where autocorrelated relaxation arises predominantly from temporal fluctuations of the CSA tensor. In our experimental work, the dipolar ^{15}N–^{1}H interactions tend to mask CSA effects. The indirect evaluation of the antisymmetric part of the CSA tensor would then become more tractable. As explained in the last section, this could be achieved by replacing the proton by a deuteron in order to quench the dominant dipolar relaxation in an X-^{1}H spin pair. Alternatively, one could focus attention on a homonuclear system such as the pair $^{13}C^{\text{ali}}$–^{13}CO.

Furthermore, one could imagine exploring anti-CSA tensor components of nuclei located in biomolecules such as polypeptides or small proteins. According to Buckingham's rules,[21] backbone nuclei could have anti-CSA tensor components that depend on the secondary structures such as alpha-helices, beta-sheets, or random coils. To accelerate overall tumbling rates, the proteins could be encapsulated in reversed micelles immersed in low-viscosity solvents.[43,44] Pending experimental evidence, the present work indicates that one can obtain at least a rough estimate of the magnitude of anti-CSA components *in silico*.

ACKNOWLEDGMENTS

We thank Dr. Fabien Ferrage and Dr. Daniel Abergel for very fruitful discussions. Dr. Eric Guittet and financial support from the TGE RMN THC (Grant No. Fr3050) for conducting the research on a 22.32 T (950 MHz) spectrometer are gratefully acknowledged. This work was supported by the European Union (Integrated Infrastucture Initiative under Contract No. RII3-026145 and Joint Research Activity JRA1 under Contract No. 026145), the Centre National de la Recherche Scientifique (CNRS, France), the Agence Nationale pour la Recherche (ANR, France), the Fonds National de la Recherche Scientifique (FNRS, Switzerland) (Grant No. 200020_124694/1), and the Commission pour la Technologie et l'Innovation (CTI, Switzerland) (Grant No. 9991.1 PFIW-IW).

[1] A. G. Palmer, Chem. Rev. (Washington, D.C.) **104**, 3623 (2004).
[2] A. Cavalli, X. Salvatella, C. M. Dobson, and M. Vendruscolo, Proc. Natl. Acad. Sci. U.S.A. **104**, 9615 (2007).

[3] L. E. Kay, D. A. Torchia, and A. Bax, Biochemistry **28**, 8972 (1989).
[4] A. Dhulesia, D. Abergel, and G. Bodenhausen, J. Chem. Phys. **129**, 095107 (2008).
[5] V. Calandrini, D. Abergel, and G. Kneller, J. Chem. Phys. **128**, 145102 (2008).
[6] B. Halle, J. Chem. Phys. **131**, 224507 (2009).
[7] Y. Goddard, J.-P. Korb, and R. G. Bryant, J. Chem. Phys. **126**, 175105 (2007).
[8] F. Kateb, D. Abergel, Y. Blouquit, P. Duchambon, C. T. Craescu, and G. Bodenhausen, Biochemistry **45**, 15011 (2006).
[9] R. Paquin, F. Ferrage, F. A. A. Mulder, M. Akke, and G. Bodenhausen, J. Am. Chem. Soc. **130**, 15805 (2008).
[10] M. Mori, F. Kateb, G. Bodenhausen, M. Piccioli, and D. Abergel, J. Am. Chem. Soc. **132**, 3594 (2010).
[11] A. L. Hansen and H. M. Al-Hashimi, J. Am. Chem. Soc. **129**, 16072 (2007).
[12] D. M. Grant, in *Encyclopedia of Nuclear Magnetic Resonance*, edited by D. M. Grant and R. K. Harris (Wiley, Chichester, 1996), Vol. 2, p. 1298.
[13] F. A. L. Anet and D. O'Leary, Concepts Magn. Reson. **3**, 193 (1991); **4**, 35 (1992).
[14] J. S. Blicharski, Z. Naturforsch. A **27**, 1456 (1972).
[15] R. M. Lynden-Bell, Mol. Phys. **29**, 301 (1975).
[16] H. W. Spiess, in *NMR Basic Principles and Progress*, edited by P. Diehl, E. Fluck, and R. Kosfeld (Springer-Verlag, New York, 1978), Vol. 15.
[17] M. T. Chenon, C. Coupry, and L. G. Werbelow, J. Phys. Chem. **96**, 561 (1992).
[18] F. A. Anet, D. O'Leary, C. G. Wade, and R. D. Johnson, Chem. Phys. Lett. **171**, 401 (1990).
[19] J. Kowalewski and L. Werbelow, J. Magn. Reson. **128**, 144 (1997).
[20] S. Wi and L. Frydman, J. Chem. Phys. **116**, 1551 (2002).
[21] A. D. Buckingham and S. Malm, Mol. Phys. **22**, 1127 (1971).
[22] B. J. Wylie, L. J. Sperling, H. L. Frericks, G. J. Shah, W. T. Franks, and C. M. Rienstra, J. Am. Chem. Soc. **129**, 5318 (2007).
[23] B. J. Wylie and C. M. Rienstra, J. Chem. Phys. **128**, 052207 (2008).
[24] K. Loth, P. Pelupessy, and G. Bodenhausen, J. Am. Chem. Soc. **127**, 6062 (2005).
[25] A. Ramamoorthy, C. H. Wu, and S. J. Opella, J. Am. Chem. Soc. **119**, 10479 (1997).
[26] D. Massiot, F. Fayon, M. Capron, I. King, S. Le Calvé, B. Alonso, J.-O. Durand, B. Bujoli, Z. Gan, and G. Hoatson, Magn. Reson. Chem. **40**, 70 (2002).
[27] P. Giannozzi, S. Baroni, N. Bonini, M. Calandra, R. Car, C. Cavazzoni, D. Ceresoli, G. L. Chiarotti, M. Cococcioni, I. Dabo, A. Dal Corso, S. de Gironcoli, S. Fabris, G. Fratesi, R. Gebauer, U. Gerstmann, C. Gougoussis, A. Kokalj, M. Lazzeri, L. Martin-Samos, N. Marzari, F. Mauri, R. Mazzarello, S. Paolini, A. Pasquarello, L. Paulatto, C. Sbraccia, S. Scandolo, G. Sclauzero, A. P. Seitsonen, A. Smogunov, P. Umari, and R. M. Wentzcovitch, J. Phys. Condens. Matter **21**, 395502 (2009); See http://www.quantum-espresso.org/.
[28] C. J. Pickard and F. Mauri, Phys. Rev. B **63**, 245101 (2001).
[29] Ch. B. Hübschle, M. Messerschmidt, and P. Luger, Cryst. Res. Technol. **39**, 274 (2004).
[30] C. Gervais, R. Dupree, K. J. Pike, C. Bonhomme, M. Profeta, C. J. Pickard, and F. Mauri, J. Phys. Chem. A **109**, 6960 (2005).
[31] C. Gervais, C. Coelho, T. Azais, J. Maquet, G. Laurent, F. Pourpoint, C. Bonhomme, P. Florian, B. Alonso, G. Guerrero, P. H. Mutin, and F. Mauri, J. Magn. Reson. **187**, 131 (2007).
[32] M. Goldman, J. Magn. Reson. **60**, 437 (1984).
[33] G. Lipari and A. Szabo, J. Am. Chem. Soc. **104**, 4546 (1982); **104**, 4559 (1982).
[34] J. Cavanagh, W. J. Fairbrother, A. G. Palmer, M. Rance, and N. J. Skelton, *Protein NMR Spectroscopy: Principles and Practice*, 2nd ed. (Academic, San Diego, 2007).
[35] P. Pelupessy, G. M. Espallargas, and G. Bodenhausen, J. Magn. Reson. **161**, 258 (2003).
[36] P. Pelupessy, F. Ferrage, and G. Bodenhausen, J. Chem. Phys. **126**, 134508 (2007).
[37] F. Ferrage, A. Piserchio, D. Cowburn, and R. Ghose, J. Magn. Reson. **192**, 302 (2008).
[38] F. Ferrage, D. Cowburn, and R. Ghose, J. Am. Chem. Soc. **131**, 6048 (2009).
[39] M. Findeisen, T. Brand, and S. Berger, Magn. Reson. Chem. **45**, 175 (2007).
[40] See supplementary material at http://dx.doi.org/10.1063/1.34457777 for more details about relaxation experiments (relaxation curves, rates, and results about thermal effects of pulse sequences) and further graphical results obtained using the model A (for different values of the distance r_{NH}, the angle β, or the eigenvalues δ_{xx}, δ_{yy}, δ_{zz}) and the model B (for $\tau_{int}=0$, 100 200 ps).
[41] J. B. Hall and D. Fushman, J. Am. Chem. Soc. **128**, 7855 (2006).
[42] P. Damberg, J. Jarvet, and A. Graslund, J. Am. Chem. Soc. **127**, 1995 (2005).
[43] A. J. Wand, M. R. Ehrhardt, and P. F. Flynn, Proc. Natl. Acad. Sci. U.S.A. **95**, 15299 (1998).
[44] Z. Shi, R. W. Peterson, and A. J. Wand, Langmuir **21**, 10632 (2005).